Optica Applicata, Vol. LV, No. 1, 2025
DOI: 10.37190/oa/200522

Investigation of novel SMF-capillary-NCF-SMF sensor for simultaneous measurement of NH_3 concentration and temperature

Feng Zhu[1], Hengyang Zhao[1], Xiaoxiao Xu[1], Zetian Liu[2], Chuanlu Deng[2,*]

[1]State Grid Anhui Electrical Power Research Institute, Hefei, China

[2]Key Laboratory of Specialty Fiber Optics and Optical Access Networks, Joint International Research Laboratory of Specialty Fiber Optics and Advanced Communication, Shanghai Institute for Advanced Communication and Data Science, Shanghai University, Shanghai

*Corresponding author: chuanludeng@163.com

A dual parameter fiber optic sensor is proposed, which is based on a cascade single mode fiber (SMF)-capillary-no core fiber (NCF)-SMF (SCNS) structure. The sensor introduces a capillary to the conventional SMF-NCF-SMF (SNS) structure, which improves the excitation co-efficient of the higher order modes in the NCF. The optimized ZnO film thickness of the SCNS sensor is 100 nm by simulation, which can enhance the sensitivity of the sensor greatly. The experimental results show that the resonant wavelength has different sensitivities to NH_3 concentration and temperature. The maximum NH_3 concentration sensitivity is 35.52 pm/ppm, with a detection limit of 2.309 ppm, and the maximum temperature sensitivity is 25.85 pm/°C. Based on the different spectral responses, a cross-matrix is developed to enable the simultaneous measurement of temperature and NH_3 concentration.

Keywords: fiber optic sensor, dual parameter sensing, NH_3 concentration, temperature, cross-matrix calibration.

1. Introduction

Ammonia (NH_3) is a chemical substance, which has been widely used in significant fields such as industry and agriculture [1]. However, long-term exposure to a certain concentration of NH_3 may cause staff to experience symptoms such as difficult breathing, dizziness, and even swelling of the lungs, which can be fatal in severe cases [2-5]. The occupational safety health act (OSHA) states that humans should not work in environments with NH_3 concentration exceeding 25 ppm for more than 8 hours and in environments with concentration exceeding 35 ppm for more than 15 minutes [6]. Therefore, the detection of NH_3 concentration is of great importance to ensure the safety of production and life.

Fiber optic sensors (FOS) have many advantages such as electromagnetic interference immunity, compact structure and real-time detection capabilities, demonstrating vast potential in the field of gas detection [7]. To detect NH_3 concentration, the gas-sensitive material is usually coated on the FOS [8-10]. The change in NH_3 concentration causes a change in the refractive index of the sensitive film, resulting in a shift in the spectrum of the sensor, which realize the detection of gas concentration. In recent years, extensive research has been conducted on various sensitive materials and diverse fiber sensing structures. In 2018, FU *et al*. [11] fabricated graphene oxide and zinc oxide (ZnO) nanoparticles on the tapered region of a tapered multi-core fiber for NH_3 concentration sensing. The sensor exhibited a high sensitivity of up to 31 pm/ppm for NH_3 concentrations ranging from 4 to 140 ppm. In 2022. ANSARI *et al*. [12] applied a layer of silane gel on a tapered multimode fiber as a sensitive material for NH_3 detection. When the waist diameter of the tapered fiber reached 4 μm, the sensor has achieved a sensitivity of 14.8 pm/ppm. In 2023, LI *et al*. [13] developed a fiber Mach–Zehnder interferometer based on an etched thin-core fiber coated with a film of graphene/polyaniline for NH_3 concentration detection. The sensor demonstrated a sensitivity of –27.8 pm/ppm within a range of 0–100 ppm.

These research findings not only enhance the sensitivity and efficiency of NH_3 detection but also provide novel sensor design idea. However, the integration of specially treated fiber structures with sensitive materials to achieve higher sensitivity is fraught with challenges in parameter control. Complex processes, including fiber tapering, etching, and fusion splicing, can introduce inconsistencies, thus compromise sensor reliability. The sensor fabricated by no core fiber (NCF) has been widely used in detecting temperature [14], humidity [15], environment refractive index [16] and other parameters. After the deposition of the sensitive material on the NCF, it can achieve a high sensitivity response to the external environment without special treatment of the optical fiber. Moreover, the capillary is a hollow-core structure that can support multiple modes of light transmission [17]. In 2017, ZHANG *et al*. [18] proposed a simple sensing structure by combining a capillary with single mode fiber (SMF). The structure takes advantage of the high sensitive characteristics of the higher-order modes to environment changes, achieving a maximum sensitivity of refractive index (1.3360–1.4365) of 1684 nm/RIU. A new cascaded structure composed of NCF and capillary can be adopted in realizing simultaneous measurement of NH_3 concentration and temperature. This design sensor has not yet been investigated.

In this paper, a FOS based on the SMF-capillary-NCF-SMF (SCNS) structure is proposed for the simultaneous detection of NH_3 concentration and temperature. In theory, the NCF structure introduces multimode interference (MMI), and the capillary improves the mode excitation coefficients of the higher-order modes in the NCF, enhancing the multimode interference effect further. Based on the principle of MMI, NH_3 concentration and temperature changes cause different shifts of the resonant wavelength experimentally. Therefore, the different responses can be used to construct a cross-matrix, which enables temperature and NH_3 concentration simultaneous detection.

2. Theory

The schematic of the proposed sensor based on the SCNS structure is shown in Fig. 1, and the detailed structural parameters is provided in Table 1. Due to the core mismatch introduced by the capillary, the incident light diffuses as it propagates from SMF1 to the capillary. Upon reaching the interface between the capillary and the NCF, this diffused light serves as the input to the NCF, exciting a range of higher-order modes. Owing to the fact that the refractive index of ZnO is higher than that of NCF, the total reflection condition is broken, and part of the transmitted light leaks into the ZnO film. Therefore, when the refractive index of ZnO film changes, the interference spectrum generated by multi-mode interference in NCF will undergo a shift.

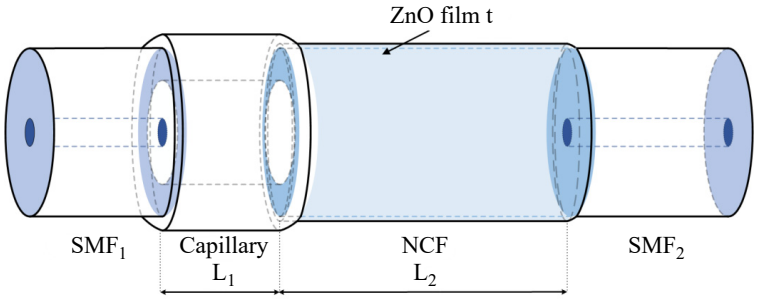

Fig. 1. Schematic diagram of the SCNS sensor.

T a b l e 1. Structure parameters of the SCNS sensor.

	Length [μm]	Core diameter [μm]	Core refractive index	Cladding diameter [μm]	Cladding refractive index
SMF	/	8	1.4681	125	1.4628
Capillary	L_1	100	1	160	1.4
NCF	L_2	/	/	125	1.444

The NCF can be regarded as the core, and the ZnO film and air can be regarded as the 1st and 2nd cladding, respectively. Since NCF is an ideal circularly symmetric structure, the higher-order mode LP_{0m} is excited in the NCF after eccentricity-free fusion splicing [19]. The input optical field is denoted as $E(r, 0)$ and the m-th order mode field distribution in NCF is denoted as $\psi_m(r)$. According to the electromagnetic field continuity condition, the input optical field of the NCF can be expressed as

$$E(r, 0) = \sum_{m=1}^{M} c_m \psi_m(r) \tag{1}$$

where r is the radius of the NCF, M is the number of LP_{0m} present in the NCF, and c_m is the excitation coefficient of the m-th order higher-order mode, which can be calculated by integrating the overlap of $\psi_m(r)$ with $E(r, 0)$ [20]:

$$c_m = \frac{\int_0^{\infty} E(r,0)\psi_m(r)\,r\,\mathrm{d}r}{\int_0^{\infty} \psi_m(r)\psi_m(r)\,r\,\mathrm{d}r} \tag{2}$$

When the inner and outer diameters of capillary are 100 and 160 μm, respectively, its beam propagation simulated is as shown in Fig. 2(a) and (b). The optical field diameter reaches a maximum at a capillary length L_1 of 250 μm, but further increase of the capillary length has little effect on the optical field diameter. The introduction of

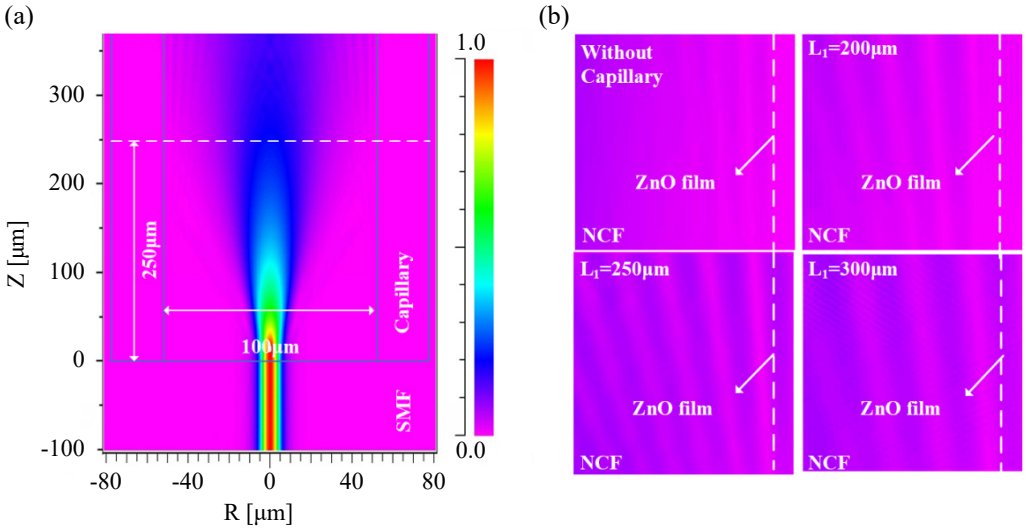

Fig. 2. (a) Simulation result of light field diffusion in NCF, and (b) the beam propagation simulation results of the ZnO film coated on NCF.

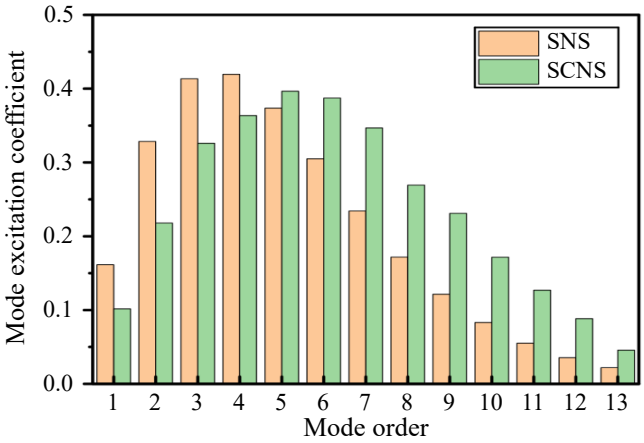

Fig. 3. Mode excitation coefficients of NCF in SNS and SCNS structure.

the capillary enhances the light energy within the ZnO film, thus increasing the sensitivity to the refractive index of the film.

The mode excitation coefficients of NCF in SCNS structure and SNS structure are shown in Fig. 3. The mode excitation coefficients reach a maximum at mode order $m = 4$ and $m = 5$ in the two structure, with maximum values of 0.4194 and 0.3964, respectively. In the SCNS structure, the mode excitation coefficients of the NCF are greater than those in the SNS structure when the mode order $m > 5$. Simulation results indicate that the SCNS structure supports a higher proportion of higher-order modes compared to the SNS structure. Generally, the mode orders involved in mode interference are higher, resulting in increased sensitivity to changes in the external environment.

2.1. Principle of NH_3 concentration sensing

As light transmits into the NCF and diffuses to the interface with the ZnO film, total internal reflection is compromised due to the higher refractive index of ZnO film, causing some light to leak into the film [21]. Due to the redox reaction, when the ZnO surface is in contact with NH_3 [22], its conductivity changes, and this change affects the refractive index of the ZnO film, which in turn affects the mode distribution in the NCF and causes a drift in the transmission spectrum. Based on the self-imaging effect of the NCF, the optical field intensity is maximized at the self-imaging length. In the previous study, the self-imaging length of the NCF was calculated to be 58.85 mm [23], where the multimode interference coupling coefficient is the highest. Therefore, choosing the NCF length L_2 of 58.85 mm can achieve the best sensing performance.

The transmission spectra of the SCNS sensing structure coated without and with ZnO film are plotted in Fig. 4. After the ZnO film with thickness of 100 nm is coated on the NCF surface, the transmission spectral loss slightly increases and the overall waveform shows a blue shift. The self-imaging peak wavelength λ_{self} of NCF shifts from 1557.25 to 1510.53 nm, and the self-imaging point peak also decreases slightly.

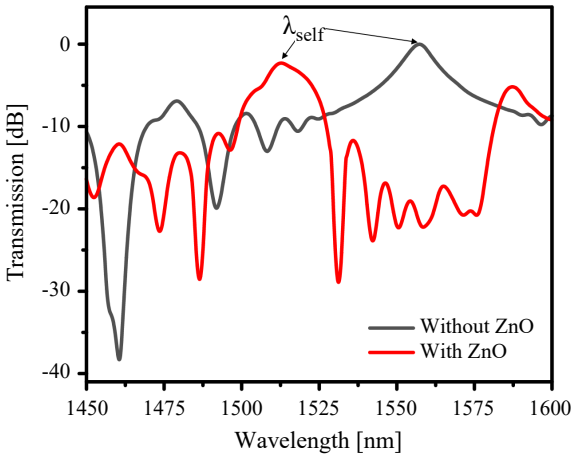

Fig. 4. Transmission spectrum of SCNS structure coated with and without ZnO film.

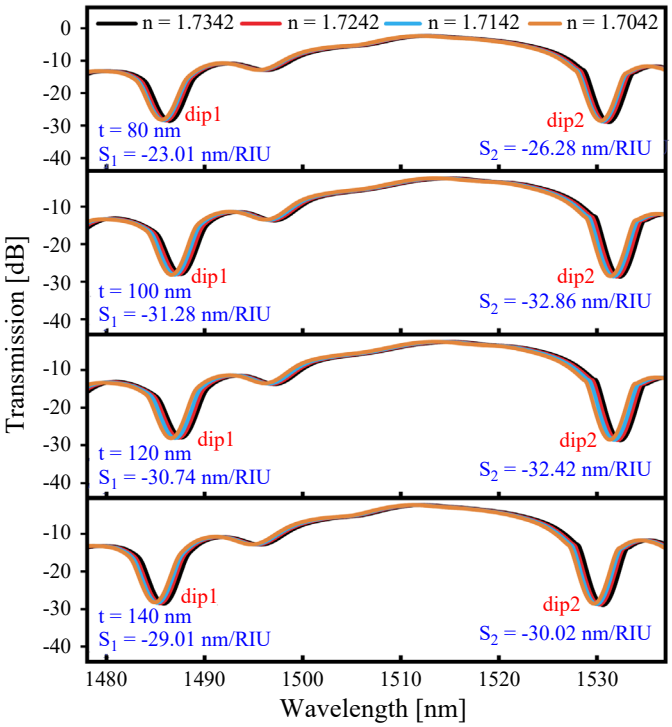

Fig. 5. Simulated transmission spectrum response of the SCNS sensor with different ZnO film thickness.

It is because that the refractive index of the ZnO film is much higher than that of NCF, breaking the total internal reflection and causing light to leak into the ZnO film, thus leading to absorption loss. Additionally, the film's refractive index affects the modes effective refractive index of NCF, causing a blue shift in the transmission spectrum.

The resonance wavelength shift at dip in Fig. 4 with NH_3 concentration is simulated. Since the refractive index of the ZnO film is correlated with NH_3 concentration, the sensor's NH_3 concentration response can be modeled by adjusting the refractive index of the film. The sensitivity of the sensor is simulated by varying the thickness of ZnO film range from 80 to 140 nm, the results of which is shown in Fig. 5. The results show that the sensitivity tends to increase and then decrease as the thickness of the ZnO film increases. The highest sensitivity has been obtained at the thickness of the film of 100 nm, with sensitivities of 31.28 and 32.86 nm/RIU for dip1 and dip2, respectively.

2.2. Temperature sensitivity characteristics

The fiber structure itself is subject to thermal expansion and thermo-optic effects. The capillary and NCF is composed of quartz material, and its thermo-optic coefficient v is about 1.1×10^{-5} °C^{-1} and its thermal expansion coefficient ζ is about 5×10^{-7} °C^{-1} in

the room temperature [24]. The size and refractive index of the capillary and NCF changes with the environment temperature as shown in the following equations:

$$\begin{aligned} n' &= (1 + v\Delta T)n \\ D' &= (1 + \zeta\Delta T)D \\ L' &= (1 + \zeta\Delta T)L \end{aligned} \tag{3}$$

where ΔT is the change in ambient temperature, n, D, and L are the initial refractive index, diameter, and length of the optical fiber, and n', D', and L' are the refractive index, diameter and length of the optical fiber after the temperature change, respectively.

As a result, the refractive index and length of capillary and NCF are prone to change with fluctuations in environmental temperature, which in turn affects the sensing spectrum. The transmission spectral response of the SCNS sensing structure at a range of environment temperature from 0 to 60 °C is simulated, as shown in Fig. 6. The dip1 and dip2, which have the largest contrast in the transmission spectrum, are selected as research point. The temperature sensitivity corresponding to dip1 and dip2 can be obtained as 23.71 and 20.01 pm/°C, respectively.

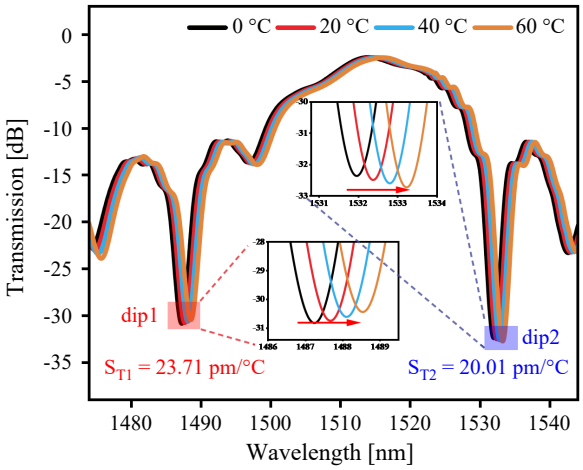

Fig. 6. Simulation of the influence of temperature on the transmission spectrum.

Since the SCNS sensor has different sensitivities to concentration and temperature, it can measure concentration and temperature simultaneously by observing the wavelength shift of the dips in the transmission spectrum.

3. Sensor fabrication and experimental setup

To precisely control the capillary and NCF length, the manual mode of a fiber optic fusion splicer (FITEL, S179) is used to fuse the optical fiber and capillary in the SCNS structure.

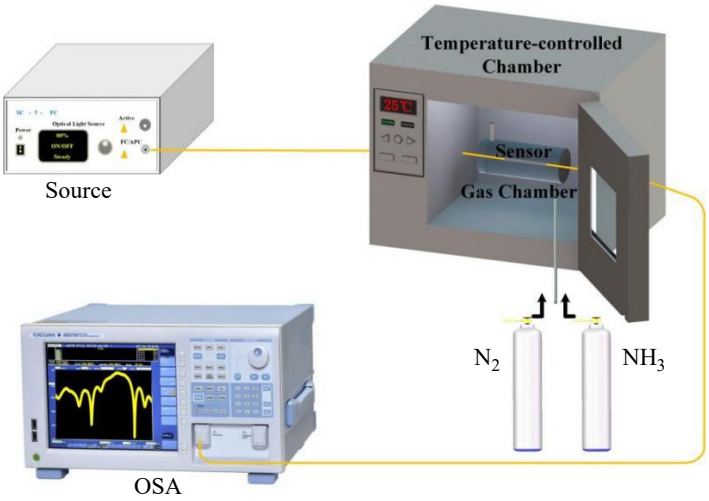

Fig. 7. Schematic diagram of the experimental setup.

During the capillary fusion, a discharge intensity of 40 bit and a duration of 100 ms are applied to avoid structure collapse and reduce fusion loss to a minimum. The deposition of zinc oxide films on the NCF surface is performed using an ALD system (Beneq, TFS200). The thickness of the film reaches 100 nm after 500 depositions at 200 °C.

A schematic diagram of the gas detection system is shown in Fig. 7. The broad-band light output from the light source (YSL, SC-5-FC) is transmitted into the sensor, and the spectrum transmitted from the sensor is directly output to the spectrometer (Yokogawa, AQ6370D). The gas concentration in the gas chamber can be controlled by changing the NH_3 gas cylinders with different concentrations. The environmental temperature is precisely controlled by a temperature-controlled chamber (Espec, GPG-4).

4. Results and discussion

4.1. NH_3 concentration sensing response

During the NH_3 concentration test, the gas chamber outlet is connected to the external environment. After cleaning the gas chamber with high purity N_2, different concentrations of NH_3 are introduced from the inlet, and the spectral response is obtained using a spectrometer, the results of which are demonstrated in Fig. 8. As the NH_3 concentration is increased from 0 to 40.4 ppm, the transmission spectrum undergoes a blue shift. Four different interference dips with relatively high contrast are identified as dip1, dip2, dip3, and dip4, with respective contrasts of 9.59, 22.65, 6.01 and 9.21 dB.

The experiment is repeated several times and a linear fit is performed by taking the mean of the wavelength values of the four dips at different NH_3 concentrations, as shown in Fig. 9. The corresponding sensitivities for NH_3 concentration for the four dips are determined to be –33.02, –35.52, –31.96 and –27.53 pm/ppm, with linear co-

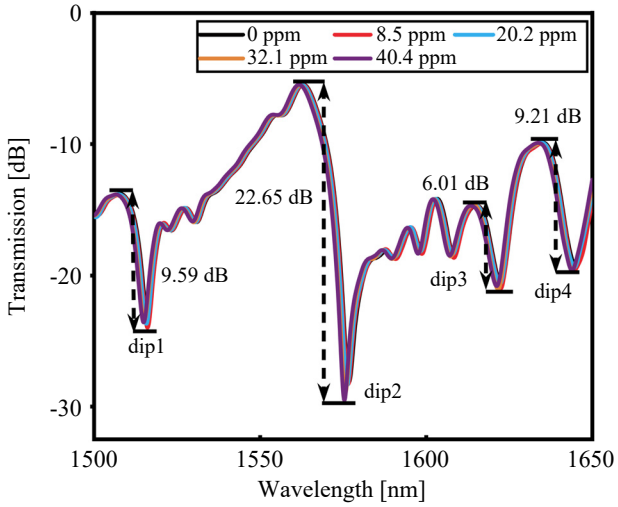

Fig. 8. The response of transmission spectrum at different NH_3 concentrations.

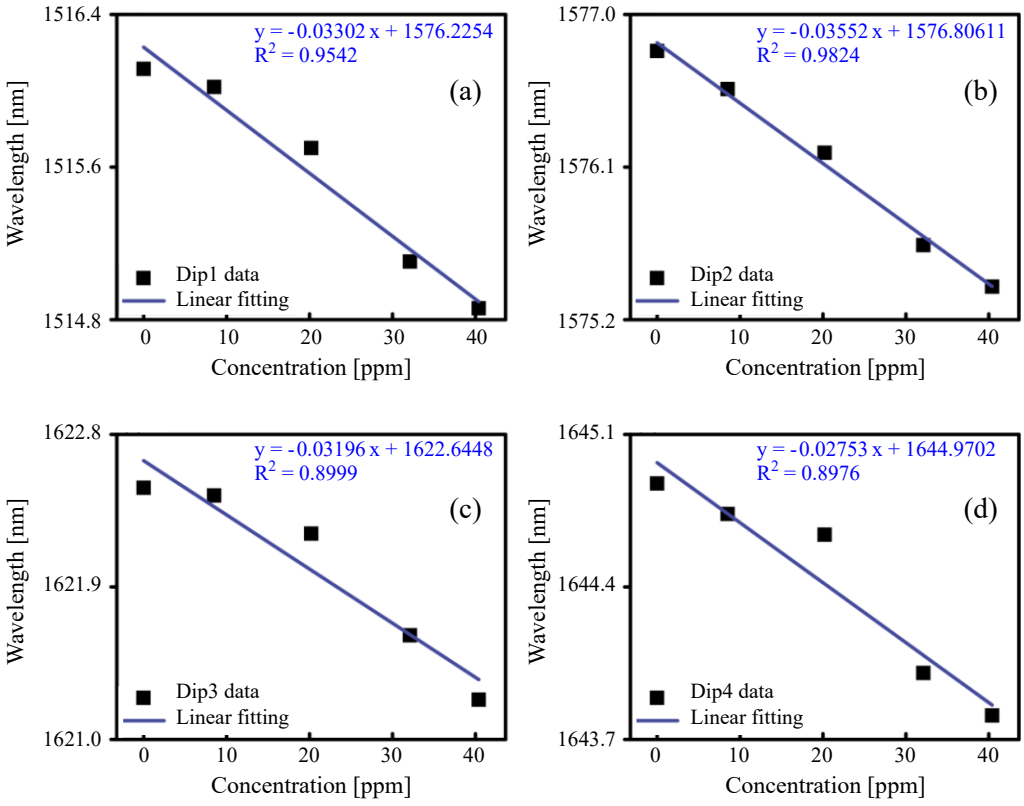

Fig. 9. The linear fitting results for NH_3 concentration. (a) dip1, (b) dip2, (c) dip3, and (d) dip4.

efficients of 0.9542, 0.9843, 0.8999, 0.8976, and 0.8976, respectively. It is observed that the greater the contrast of the dip, the higher the NH_3 concentration sensitivity. The deeper dip intensifies the interference between the core mode and higher-order cladding mode [25], promoting greater leakage of core modes into the cladding. This results in decrease of transmitted light intensity and improves the sensitivity to variations in NH_3 concentration.

Selecting the higher contrast dip1 and dip2 as references gives the SCNS sensors more stable interferometric effects and higher sensitivity. Furthermore, the limit of detection (LOD) of dip2 for NH_3 concentration can be calculated as 2.309 ppm by the formula LOD = $3\sigma/K$ [26], where σ (defined as the standard deviation of the fitting curve) is 0.02734 nm and K (defined as the sensor's sensitivity) is 35.52 pm/ppm.

4.2. Temperature sensing response

In order to avoid the effect of temperature fluctuation, the temperature in the chamber is monitored in real time using a thermocouple (Fluke, 54IIB). When the temperature is stabilized to 0, 20, 40, and 60 °C, respectively, the spectral response of the SCNS sensor is recorded, as shown in Fig. 10. It is clear that the transmission spectrum undergoes a red shift when the temperature increases. The responses of dip1 and dip2 of the transmission spectrum are locally enlarged, as illustrated in Figs. 11(a) and (b), respectively. Correspondingly, a linear fit to dip1 and dip2 is performed, as illustrated in Figs. 11(c) and (d), respectively. Therefore, the temperature sensitivities are calculated to be 25.85 and 20.25 pm/°C, with linearity coefficients of 0.9693 and 0.9860, respectively. The size and refractive index of the fiber and ZnO film [27] are influenced by the thermal expansion and thermo-optic effect. These combined effects cause a red shift in the spectrum as the environmental temperature rises from 0 to 60 °C, which is consistent with the simulation results.

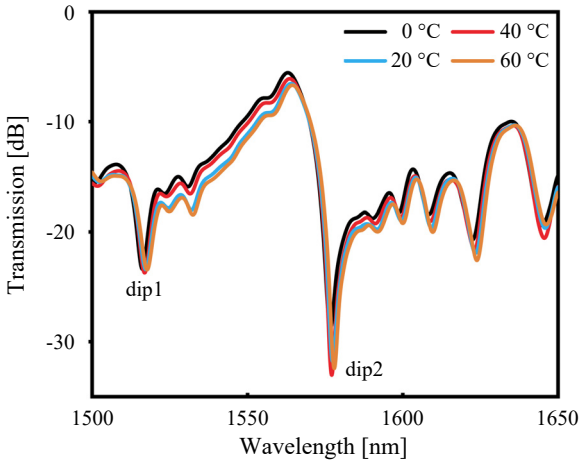

Fig. 10. The response of transmission spectrum at different temperature.

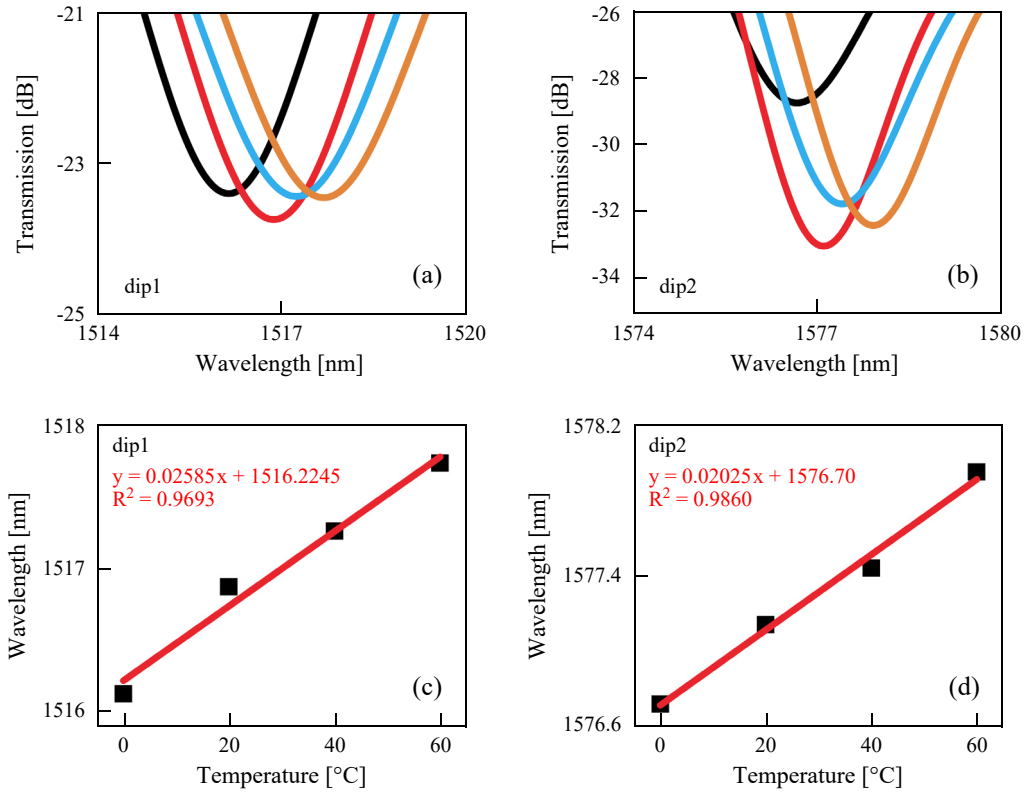

Fig. 11. Local temperature response for (a) dip1 and (b) dip2; linear fitting results for (c) dip1 and (d) dip2.

The SCNS sensor has different responses to temperature and NH_3 concentration, thus it is possible to build a cross-matrix to achieve dual parametric sensing of temperature and concentration.

4.3. Simultaneous measurement of NH_3 concentration and temperature

The change of NH_3 concentration can be expressed as ΔC, and the change of environment temperature as ΔT. When both NH_3 concentration and environment temperature simultaneously change, the wavelength shifts of dip1 and dip2 in the transmission spectrum can be expressed as follows [28]:

$$\begin{cases} \Delta\lambda_{\text{dip1}} = S_{C1}\Delta C + S_{T1}\Delta T \\ \Delta\lambda_{\text{dip2}} = S_{C2}\Delta C + S_{T2}\Delta T \end{cases} \tag{4}$$

where $\Delta\lambda_{\text{dip1}}$ and $\Delta\lambda_{\text{dip2}}$ are the respective wavelength shift quantities of the two distinctive dips. S_{C1} and S_{T1} are denoted as the NH_3 concentration and temperature sen-

sitivity for dip1, while S_{C2} and S_{T2} are corresponded to the NH_3 concentration and temperature sensitivity for dip2, respectively.

Therefore, the change in NH_3 concentration and environment temperature can be expressed as

$$\begin{bmatrix} \Delta C \\ \Delta T \end{bmatrix} = \frac{1}{S_{T2} \times S_{C1} - S_{T1} \times S_{C2}} \begin{bmatrix} S_{T2} & -S_{C2} \\ -S_{T1} & S_{C1} \end{bmatrix} \begin{bmatrix} \Delta\lambda_{dip1} \\ \Delta\lambda_{dip2} \end{bmatrix} \tag{5}$$

By substituting the sensitivity values of NH_3 concentration and temperature obtained from the transmission spectrum into the above matrix, a temperature calibration sensing matrix is obtained:

$$\begin{bmatrix} \Delta C \\ \Delta T \end{bmatrix} = \frac{1}{249.54} \begin{bmatrix} 20.25 & 35.52 \\ -25.85 & -33.02 \end{bmatrix} \begin{bmatrix} \Delta\lambda_{dip1} \\ \Delta\lambda_{dip2} \end{bmatrix} \tag{6}$$

As a result, simultaneous sensing of both NH_3 concentration and temperature can be achieved by monitoring the wavelength drift of dip1 and dip2.

5. Conclusions

In this study, a dual parameter fiber optic sensor based on the SCNS structure is proposed for simultaneous sensing of NH_3 concentration and temperature. The sensing principle of NH_3 concentration and temperature of the SCNS structure is deeply analyzed in theory, and the optimum structural parameters are determined through numerical simulation. In the experiment, the NH_3 concentration and temperature sensing test systems are built. The SCNS sensor has achieved a high sensitivity of 35.52 pm/ppm over the NH_3 concentration range from 0–40.4 ppm, with a detection limit of 2.309 ppm. Moreover, the sensor has achieved a maximum temperature sensitivity of 25.85 pm/°C within the range of 0–60 °C. With the different responses of the transmission spectrum to NH_3 concentration and temperature, a cross-matrix can be established to achieve the dual-parameter detection of NH_3 concentration and temperature. The new method for multi-parameter gas sensing will be widely used in industry and agriculture.

Funding
The State Grid Anhui Electric Power Co., Ltd. Technology Project (52120523000J).

References

[1] KWAK D., LEI Y., MARIC R., *Ammonia gas sensors: A comprehensive review*, Talanta **204**, 2019: 713-730. https://doi.org/10.1016/j.talanta.2019.06.034

[2] XIONG Y., XU W., DING D., LU W., ZHU L., ZHU Z., WANG Y., XUE Q., *Ultra-sensitive NH_3 sensor based on flower-shaped SnS_2 nanostructures with sub-ppm detection ability*, Journal of Hazardous Materials **341**, 2018: 159-167. https://doi.org/10.1016/j.jhazmat.2017.07.060

[3] YU C.B., WU Y., LIU X.L., YAO B.C., FU F., GONG Y., RAO Y.J., CHEN Y.F., *Graphene oxide deposited microfiber knot resonator for gas sensing*, Optical Materials Express **6**(3), 2016: 727-733. https://doi.org/10.1364/OME.6.000727

[4] YEBO N.A., SREE S.P., LEVRAU E., DETAVERNIER C., HENS Z., MARTENS J.A., BAETS R., *Selective and reversible ammonia gas detection with nanoporous film functionalized silicon photonic micro-ring resonator*, Optics Express **20**(11), 2012: 11855-11862. https://doi.org/10.1364/OE.20.011855

[5] TIMMER B., OLTHUIS W., VAN DEN BERG A., *Ammonia sensors and their applications—a review*, Sensors and Actuators B: Chemical **107**(2), 2005: 666-677. https://doi.org/10.1016/j.snb.2004.11.054

[6] LIANG Q., LI D., GAO S., JIANG D., ZHAO J., QIN J., HOU J., *Room-temperature NH_3 sensors with high sensitivity and short response/recovery times*, Chinese Science Bulletin **59**, 2014: 447-451. https://doi.org/10.1007/s11434-013-0018-3

[7] ASHRY I., MAO Y., WANG B., HVEDING F., BUKHAMSIN A.Y., NG T.K., OOI B.S., *A review of distributed fiber–optic sensing in the oil and gas industry*, Journal of Lightwave Technology **40**(5), 2022: 1407-1431. https://doi.org/10.1109/JLT.2021.3135653

[8] HAO T., CHIANG K.S., *Graphene-based ammonia-gas sensor using in-fiber Mach-Zehnder interferometer*, IEEE Photonics Technology Letters **29**(23), 2017: 2035-2038. https://doi.org/10.1109/LPT.2017.2761981

[9] RONG D., MENG G., FANG X., YOU L., DENG Z., *Delafossite $AgAlO_2$ modified long-period grating for highly-sensitive ammonia sensor*, Optics Express **29**(25), 2021: 42005-42019. https://doi.org/10.1364/OE.438177

[10] YU C., WU Y., LIU X., FU F., GONG Y., RAO Y.-J., CHEN Y., *Miniature fiber-optic NH_3 gas sensor based on Pt nanoparticle-incorporated graphene oxide*, Sensors and Actuators B: Chemical **244**, 2017: 107-113. https://doi.org/10.1016/j.snb.2016.12.126

[11] FU H., JIANG Y., DING J., ZHANG J., ZHANG M., ZHU Y., LI H., *Zinc oxide nanoparticle incorporated graphene oxide as sensing coating for interferometric optical microfiber for ammonia gas detection*, Sensors and Actuators B: Chemical **254**, 2018: 239-247. https://doi.org/10.1016/j.snb.2017.06.067

[12] ANSARI M., MORAVVEJ-FARSHI M.K., *Dual-purpose optical fiber sensor: Relative humidity and ammonia detection*, Optics Continuum **1**(2), 2022: 335-344. https://doi.org/10.1364/OPTCON.450252

[13] LI L., XUE M., MA Q., LIU X., GU X., XIU W., YANG X., LV M., *Graphene/polyaniline film optical fiber ammonia gas sensor with excellent sensing performance*, IEEE Sensors Journal **23**(14), 2023: 15652-15659. https://doi.org/10.1109/JSEN.2023.3283963

[14] ZHAO Y., ZHAO J., ZHAO Q., *High sensitivity seawater temperature sensor based on no-core optical fiber*, Optical Fiber Technology **54**, 2020: 102115. https://doi.org/10.1016/j.yofte.2019.102115

[15] ZEBIAN H.Y., H.J. TAHER H.J., *Relative humidity sensor based on no-core multimode interferometer coated with Al_2O_3-PVA composite films*, Optical Fiber Technology **54**, 2020: 102110. https://doi.org/10.1016/j.yofte.2019.102110

[16] HU H., SONG X., HAN Q., CHANG P., ZHANG J., LIU K., DU Y., WANG H., LIU T., *High sensitivity fiber optic SPR refractive index sensor based on multimode-no-core-multimode structure*, IEEE Sensors Journal **20**(6), 2020: 2967-2975. https://doi.org/10.1109/JSEN.2019.2956559

[17] RUSSELL P.ST.J., *Photonic-crystal fibers*, Journal of Lightwave Technology **24**(12), 2006: 4729-4749. https://doi.org/10.1109/JLT.2006.885258

[18] ZHANG X., SHAO H., YANG Y., PAN H., PANG F., WANG T., *Refractometry with a Tailored sensitivity based on a single-mode-capillary-single-mode fiber structure*, IEEE Photonics Journal **9**(2), 2017: 6801908. https://doi.org/10.1109/JPHOT.2017.2690686

[19] WU Q., SEMENOVA Y., WANG P., FARRELL G., *High sensitivity SMS fiber structure based refractometer – analysis and experiment*, Optics Express **19**(9), 2011: 7937-7944. https://doi.org/10.1364/OE.19.007937

[20] LI E.B., WANG X.L., ZHANG C., *Fiber-optic temperature sensor based on interference of selective higher-order modes*, Applied Physics Letters **89**(9), 2006: 091119. https://doi.org/10.1063/1.2344835

[21] ZHU Y., FU H.W., DING J.J., LI H.D., ZHANG M., ZHANG J., LIU Y.G., *Fabrication of three-dimensional zinc oxide nanoflowers for high-sensitivity fiber-optic ammonia gas sensors*, Applied Optics **57**(27), 2018: 7924-7930. https://doi.org/10.1364/AO.57.007924

[22] CHAUDHARY D.K., MAHARJAN Y.S., SHRESTHA S., MAHARJAN S., SHRESTHA S.P., JOSHI L.P., *Sensing performance of a ZnO-based ammonia sensor*, Journal of Physical Science **33**(1), 2022: 97-108.

[23] LIU Z.T., HUANG Y., ZHU F., HE Y.Y., DENG C.L., HU C.Y., ZHANG Q., DONG Y.H., ZHANG X.B., WANG T.Y., *Simultaneous measurement of ammonia concentration and gas pressure based on fiber multi-mode and Fabry-Pérot interference*, Optics Express **32**(15), 2024: 25607-25618. https://doi.org/10.1364/OE.523067

[24] HUANG S.Y., BLAKE J.N., KIM B.Y., *Perturbation effects on mode propagation in highly elliptical core two-mode fibers*, Journal of Lightwave Technology **8**(1), 1990: 23-33. https://doi.org/10.1109/50.45925

[25] XIONG R., MENG H., YAO Q., HUANG B., LIU Y., XUE H., TAN C., HUANG X., *Simultaneous measurement of refractive index and temperature based on modal interference*, IEEE Sensors Journal **14**(8), 2014: 2524-2528. https://doi.org/10.1109/JSEN.2014.2310463

[26] LIU S.D., YANG X.Z., FENG W.L., *Hydrogen sulfide gas sensor based on copper/graphene oxide coated multi-node thin-core fiber interferometer*, Applied Optics **58**(9), 2019: 2152-2157. https://doi.org/10.1364/AO.58.002152

[27] SAHA S., MEHAN N., SREENIVAS K., GUPTA V., *Temperature dependent optical properties of (002) oriented ZnO thin film using surface plasmon resonance*, Applied Physics Letters **95**(7), 2009: 071106. https://doi.org/10.1063/1.3206954

[28] HUANG Y., QIU H., DENG C.L., LIAN Z.G., YANG Y., YU Y., HU C.Y., DONG Y.H., SHANG Y.N., ZHANG X.B., WANG T.Y., *Simultaneous measurement of magnetic field and temperature based on two anti-resonant modes in hollow core Bragg fiber*, Optics Express **29**(20), 2021: 32208-32219. https://doi.org/10.1364/OE.439444

Received December 20, 2024
in revised form January 22, 2025